Environmental Management (2013) 52:234–249
DOI 10.1007/s00267-013-0097-6

Land Surface Phenology and Land Surface Temperature Changes Along an Urban–Rural Gradient in Yangtze River Delta, China

Guifeng Han · Jianhua Xu

Received: 15 May 2012 / Accepted: 27 May 2013 / Published online: 6 June 2013

Abstract Using SPOT/VGT NDVI time series images (2002–2009) and MODIS/LST images (2002–2009) smoothed by a Savitzky–Golay filter, the land surface phenology (LSP) and land surface temperature (LST), respectively, are extracted for six cities in the Yangtze River Delta, China, including Shanghai, Hangzhou, Nanjing, Changzhou, Wuxi, and Suzhou. The trends of the averaged LSP and LST are analyzed, and the relationship between these values is revealed along the urban–rural gradient. The results show that urbanization advances the start of the growing season, postpones the end of the growing season, prolongs the growing season length (GSL), and reduces the difference between maximal NDVI and minimal NDVI in a year ($NDVI_{amp}$). More obvious changes occur in surface vegetation phenology as the urbanized area is approached. The LST drops monotonously and logarithmically along the urban–rural gradient. Urbanization generally affects the LSP of the surrounding vegetation within 6 km to the urban edge. Except for GSL, the difference in the LSP between urban and rural areas has a significant logarithmic relationship with the distance to the urban edge. In addition, there is a very strong linear relationship between the LSP and the LST along the urban–rural gradient, especially within 6 km to the urban edge. The correlations between LSP and gross domestic product and population density reveal that human activities have considerable influence on the land surface vegetation growth.

Keywords Urbanization · Land surface phenology · Land surface temperature · Urban–rural gradient · Yangtze River Delta region

G. Han (✉)
Key Laboratory of New Technology for Construction of Cities in Mountain Area of Education Ministry, College of Architecture and Urban Planning, Chongqing University, Chongqing 400045, China
e-mail: hangf@cqu.edu.cn

J. Xu
Key Laboratory of Geographic Information Science of Education Ministry, Department of Geography, East China Normal University, Shanghai 200062, China

Introduction

Urbanization is an important character of today's world development, especially in developing countries. As the process of global urbanization accelerates both in intensity and in area, there is a growing interest in understanding its implications of this process with respect to a broad set of environmental factors, including the net primary production, the biodiversity, and the climate and weather at local, regional, and global scales (Imhoff and others 2010). Vegetation is the most important type of land cover on the land surface and plays an important role in urban ecosystem structure and function. The vegetation in an urban area is first disturbed or directly removed. Then, urban forests and bushes are eradicated, and large areas of the soil surface are covered by impervious materials, such as cement and asphalt. Finally, artificial vegetation will be programmed in the urban area. Hence, it is almost impossible for an urban ecosystem to recover its original status. The continuous expansion of metropolitan regions transforms open spaces at the urban fringe from forest and agriculture into areas with increasing amounts of impervious surfaces in the form of buildings and pavement (Lee and French 2009). The results of human activities, such as discarded heat, highly diverse buildings, and large areas of

impervious surfaces, are one of the most important factors changing the local climate in city (Roetzer and others 2000). Recent studies show that the increase of impervious surface is also closely correlated with the urban heat island (UHI) effect and the associated air pollution problems (Sailor 1995; Lo and Quattrochi 2003; Yuan and Bauer 2007). As the UHI effect becomes increasingly obvious, the original vegetation in urban areas decreases rapidly (Han and others 2007), the landscape patterns change constantly (Wang and others 2006a, b; Gong and others 2006), and the species and diversity of the vegetation are eliminated (Kinzig and others 2005; Li and others 2005). All of these changes can directly or indirectly influence vegetation phenology. Phenological events have a large influence on the spatiotemporal dynamics of the carbon and water cycles (White and others 1997). The characterization of land surface vegetation phenology at regional, national, and global scales has been recognized as important for many scientific and practical applications. For example, the analysis of the start and end of the growing season (EOS) at a global scale can be an important indicator of global climate change, and the spatial variation of these values can be used to determine the regional variations of the effect caused by changing temperature and precipitation regimes (Zhou and others 2001).

Long and homogeneous phenology records with good spatial coverages are important for traditional phenology studies (Ahas and others 2002). Except for Europe and North America, however, phenology records in other countries and regions of the world are incomplete, especially in developing countries. The Chinese Phenology Network was established in 2002 based on the original 62 observation stations established by Chu Kochen in 1962 (http://www.igbp-cnc.org.cn/cpn/index.html). The scientific phenology observations were developed later in China but have experienced rapid progression in recent years (Ge and others 2010). With the development of remote sensing technology, using time series remote sensing images has gradually become one of the most common means to detect surface vegetation phenology due to the high time resolution such as AVHRR, SPOT/VGT, and MODIS (Wu and others 2008). Most phenology measurements recorded by satellite imagery are based on the NDVI time series because this value has been demonstrated to be a reliable remote sensing indicator of the start and EOS of the land surface vegetation (Li and others 2006). Recently, much research about vegetation phenology at regional, national, and global scales has been reported using long-term plant phenology data from land observation stations and coarse remote sensing images (Zheng and others 2002; de Beurs 2005; Pettorelli and others 2005; Li and others 2006; Neil and Wu 2006; Karlsen and others 2009). At small scales, however, only a few research papers have reported that the spatial different of land surface vegetation phenology along the urban–rural gradient is changed by urbanization (White and others 2002; McDonnell and others 1997). The influence of urbanization on vegetation phenology is variable. In cities such as Miami, urbanization results in the loss of 22 full days of peak season plant growth per year. In cities such as Denver, however, urbanization actually adds 11 days of vegetation productivity (Weier 2002). Although many studies have found that urbanization promotes an earlier start of the season and delays the end of the season, how urbanization affects vegetation phenology has not been completely elucidated. The Yangtze River Delta is one of the most developed regions in China, and in this region, the vigor and distribution of vegetation are evidently affected by urbanization and relevant human activities (Han and Xu 2008). However, few studies have reported the impact of urbanization on vegetation phenology. The UHI effect is one of the most important consequences of urbanization. With the development of remote sensing technology, it is easy to measure the upwelling thermal radiance. And this indirect measurement of the surface temperature is often referred to as the surface UHI (SUHI) (Roth and others 1989; Voogt and Oke 2003). The land surface temperature (LST) derived from remote sensing data has, therefore, been an important indicator of the UHI effect in the past two decades. This study aims to analyze the distribution of land surface phenology (LSP) and LST in the six major cities in the Yangtze River Delta and to compare the LSP and LST in urban and rural areas to understand changes in the LSP and the impact of the LST on the LSP along the urban–rural gradient.

Study Area and Methodology

Study Area

The Yangtze River Delta, downstream of the Yangtze River and near the sea entrance, is within the range of N29°02′–33°25′ and E118°20′–122°57′. The study area covers approximately 100,000 km^2 and contains a population of 76 million, including Shanghai city, Jiangsu province, and Zhejiang province (Fig. 1). The climate is defined as a sub-tropical humid monsoon climate with an annual average air temperature from 15 to 17 °C and an annual average precipitation of approximately 1,000–1,800 mm. In addition to crops, the dominant vegetation of the mountain area, especially in southern Zhejiang province, is evergreen broadleaf vegetation and a mixture of evergreen broadleaf vegetation and deciduous broadleaf vegetation. The slight seasonal dynamics of the NDVI of evergreen broadleaf vegetation (e.g., lower amplitudes of variation, Soudani and others 2012) has little

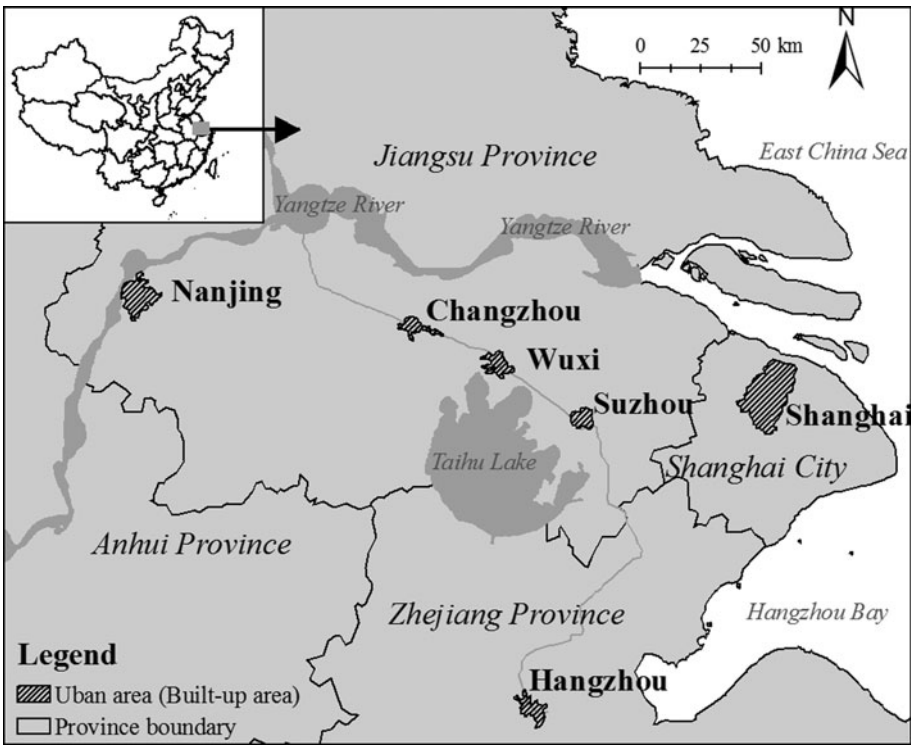

Fig. 1 The location of the study area and six urban areas

effect on comparisons between the urban area and rural area. Moreover, natural vegetation is almost replaced by cultivated vegetation in the urban area and its surrounding area. Only a few secondary forests survive in the mountain area because of the high population density and the rapid urbanization in this region. In 2003, the urbanization levels (the ratio of the urban population to the total population in a region, e.g., a city, county, or province) of Shanghai, Zhejiang province, and Jiangsu province are 77.6, 53, and 46.8 %, respectively, and are among the highest in China. The six major cities in the study are Shanghai, Hangzhou, Nanjing, Suzhou, Wuxi, and Changzhou.

Methodology

Data

The NDVI time series data from January 2002 to December 2009 selected in this study are derived from the VEGETATION (VGT) loaded on the SPOT satellites with a 1-km resolution. VGT is specially designed to detect the dynamic change in vegetation at the regional and global scales on the land surface, which can produce high-quality data for large-scale or mesoscale environmental monitoring (Xu and others 2005). The data are suited to time series analysis because the data distributed from VGT have high-precision geometric corrections (Griguolo and Mazzanti 2004). NDVI images (S10) and their corresponding status maps (SM) are downloaded from the VITO website (http://free.vgt.vito.be/home.php). The subsets are then created using the smart program (CROP_VGT, Version 2.0) written by VITO. DN values are converted to NDVI values using the formula: NDVI = DN × 0.004–0.1.

In this study, the LST is derived from MODIS data products (MOD11A2) with a 1-km resolution from 2002 to 2009, which were downloaded from the NASA website (https://wist.echo.nasa.gov). MOD11A2 is the averaged LST from MOD11A1 products over 8 days. All LST images are first transformed into the WGS1984 coordinate system based on control points on topographic maps and are then adjusted to the NDVI images using georeferencing in ArcGIS 9.3 with an error of less than one pixel (1 km).

The NDVI images are processed by the method of the maximum value composites (MVC) during each 10-day period (a dekad), as well as LST images. The MVC method can eliminate much of the error from calibration, atmospheric conditions and sensor degradation (Smith and others 1997; Tucker and others 2005). We convert these rasters (LSP and LST) to point features in the urban area (built-up area) and its surrounding area (buffer zone) to precisely reveal the trends of the LSP and LST and the relationship between these trends along the urban–rural gradient. In addition, other auxiliary data are used to extract the urban edge (the edge of the built-up area), including digital land use maps of Shanghai, Zhejiang province and Jiangsu province produced in 2003 with a scale of 1:250,000, and MODIS Land Cover production (MOD12Q1 in 2003). Population and gross domestic

product (GDP) raster maps for 2003 are produced at a 1-km resolution by the Institute of Geographic Science and Natural Resource, Chinese Academy of Science.

Phenological Measure Extraction

The images contain a small amount of residual noise, although the time series images are processed using the MVC method. It is therefore necessary to smooth the time series images before detecting variability in the LSP and LST. In this study, the time series images are smoothed with Matlab6.5 and ArcGIS9.3, as shown in the flowchart (Fig. 2).

Moving Average Smoothing First, we must identify abnormal values including false low values and false high values. On an NDVI image, the former are identified on the SM where the cells are contaminated by cloud or scan strip. The latter are considered if a difference in the NDVI between continuous two dekads is more than 0.6 at the same location because this difference disobeys the gradual natural process of vegetating (Chen and others 2004). A moving average is used to remove the abnormal values. A period of two dekads (20 days) is selected as the best step in the moving average based on the auto-correlation analysis of 100 random samples, i.e., the raw NDVI value of an abnormal cell is replaced by the mean value of the following 20 days and the preceding 20 days.

Savitzky–Golay Smoothing Subsequently, we apply a Savitzky–Golay (SG) filtering procedure to each annual NDVI cycle, as described by Chen and others (2004), to reduce the contamination by clouds, snow, and ice. The SG smoother is a linear filter that smooths data or computes a smoothed derivative of a given order and preserves the peaks and other important features of the underlying signal; it is controlled by two parameters: SPAN and DEGREE. The SPAN is the half-width of the smoothing window. Usually, a larger value of SPAN produces a smoother result at the expense of flattening sharp peaks. The DEGREE is an integer specifying the degree of the smoothing polynomial, which is typically set in a range from 2 to 4. A smaller DEGREE will produce a smoother result but may introduce bias; a higher DEGREE will reduce the filter bias but may "over fit" the data and give a noisier result (Chen and others 2004). We select 7 SPANs (5, 7, 11, 13, 15, 19, and 25) and 3 DEGREEs (2, 3, and 4) for 10 random sample points and gain 21 span-degree combinations. Based on the fitting effect index (FI) (Chen and others 2004), the best parameters are identified as a SPAN equal to 7 and a DEGREE equal to 4 for both the NDVI and LST.

LSP Extraction We extract the key phenological measures (metrics) using the smoothed NDVI time series data. The phenological metrics can be derived from the satellite data in several ways, which ranges from simple smoothing to nonlinear inverse modeling approaches (Fisher and others 2006) that have been developed over the last 20 years. These methods were grouped into three broad categories by Reed and others (1994): threshold-based methods, trend derivative methods and inflection point methods. de Beurs (2005) made a comprehensive review of the current advances in this field before 2005 (for more information, see de Beurs 2005) and divided these approaches into four categories: threshold, derivative, transformation, and model fit. In recent years, these methods have frequently been employed or improved in many studies, and some new methods have been developed, such as the modified threshold method (Maignan and others 2008; Jönsson and others 2010; Hudson Dunn and de Beurs 2011; Dash and others 2010; Atkinson and others 2012), a low-order fit (Zhang and others 2003; Fisher and others 2006), the two-step filtering method (Sakamoto and others 2010), the sigmoidal logistic models (Garrity and

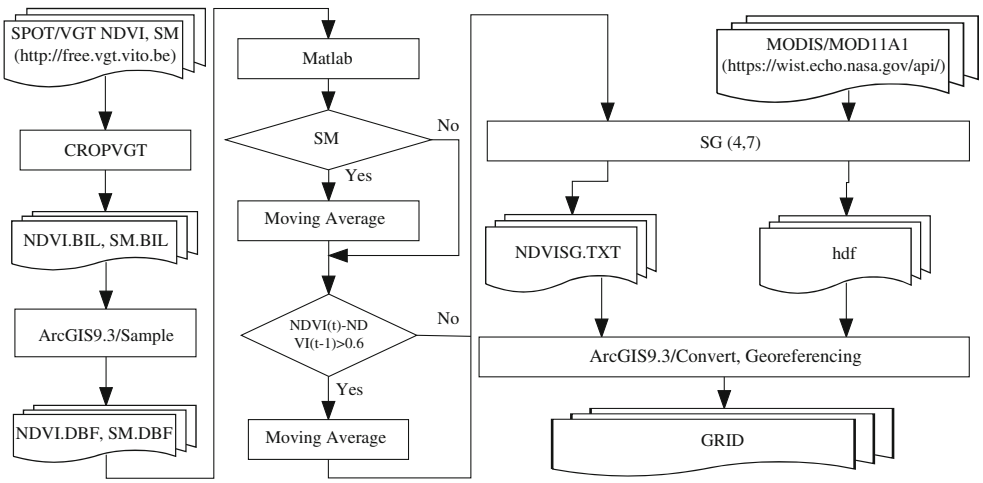

Fig. 2 Flowchart of time series images processing

others 2011), the double logistic function (Beck and others 2006; Pouliot and others 2011), the logistic model (Hufkens and others 2012), and the algorithms of the "Phenolo" package developed at the EC Joint Research Centre (Ivits and others 2012). Threshold-based methods use either a pre-defined or relative reference value to define phenology transition dates. The trend or curve derivative phenology method attempts to identify points of departure between the original vegetation temporal signal data and a derivative curve. The inflection point phenology method is based on detecting points at which the maximum curvature occurs in a plotted time series of vegetation indices (Dash and others 2010).

The characterization and analysis of land surface phenologies have advanced rapidly in recent years with the advent of more and richer data sources and a widening realization of the centrality of phenology to integrating diverse biogeophysical processes (de Beurs and Henebry 2010). However, these methods have their own advantages and shortcomings resulting from the dataset, climate conditions, ecoregions, land use/land cover, and scale, among others (Wu and others 2008). White and others (2009) estimated the time of the onset of greenness for North America using 10 methods and found that individual methods differed in the average day-of-the-year (DOY) estimates by ±60 days and in the standard deviation by ±20 days. Therefore, there are challenges in deriving phenological metrics from remote sensing. In our processing, after the raw NDVI time series data removed abnormalities by the moving average, and the data were processed by applying the SG filter (Fig. 1), a method is then applied to extract the LSP based on the point of intersection of the NDVI curve and the NDVI curve calculated by a moving average with a step of 12. The DOY of the intersection is defined as the time of the phenological event (Reed and others 1994; de Beurs 2005). Here, four primary measures are extracted from the NDVI time series data: the time of the onset of greenness (SOS), the time of the end of greenness (EOS), the growing season length (GSL), and the NDVI amplitude ($NDVI_{amp}$). The SOS and EOS define the dates at which a smoothed time series curve crosses a curve established using autoregressive moving average models. The GSL is defined as the days from the SOS to the EOS, and the $NDVI_{amp}$ is defined as the difference between the maximal NDVI and the minimal NDVI in a year, which can indicate the capacity of vigor and net primary product (NPP) of land surface vegetation well.

Buffer Zones

A series of buffers extending 0–2, 2–4, 4–6, 6–8, 8–10, 10–12, 12–14, 14–16, 16–18, and 18–20 km from the edges of the urban land cover were created for each city. The vectorial land use maps are used to extract the edges of the urban land cover. We can then calculate the mean LSP metrics, the LSTs, the population densities and the GDPs in each buffer zone in each city with the zonal statistic function in ArcGIS9.3. In addition, regression analysis is conducted to measure the trends in the LSP, the LST, the population density and the GDP, and the correlation between the LST and the LSP along the urban–rural gradient.

In each city, the mean LSP and mean LST in every buffer zone are extracted. To accurately demonstrate the difference between the urban and rural areas, LSP metrics and the LST in each city are calculated using the equation below. We can then acquire ΔSOS, ΔEOS, ΔGSL, $\Delta NDVI_{amp}$, and ΔLST, which indicate the early days of the SOS, the delayed days of the EOS, the additional days of the GSL, the decreased $NDVI_{amp}$ and the LST difference between the urban and rural areas

$$\Delta P_{ij} = P_{ij} - P_{uj},$$

where ΔP_{ij} is the difference in the phenology measures or the LST between an urban area j and its buffer zone i; P_{ij} represents the phenology measures or the LST in the buffer zone i around an urban area j; and P_{uj} represents the phenology measures or the LST in an urban area j. In addition, the differences between an urban area and rural area are fit using the least squares approach.

Results

Spatial Distribution of the LSP and LST

First, four phenology measures are extracted for each year in the study area. A similar spatial distribution pattern was found for each phenology measure from 2002 to 2009. That is, the LSP remained relatively stable during this period, regardless of the SOS, EOS, GSL, or peak NDVI. To demonstrate the slight fluctuations, 20 plots (5×5 km^2) were sampled randomly, and mean phenologies of the 20 plots are extracted for every year. The results show that, from 2002 to 2009, the SOS varied between 62 and 86 DOY, the EOS varied between 310 and 330 DOY, the GSL varied between 262 and 278 days, the peak NDVI varied between 0.32 and 0.45 and the time of the peak NDVI varied between 239 and 251 DOY. Here, we concentrate on analyzing how the LSP changes along the urban–rural gradient; therefore, we calculate the mean land surface phonology from 2002 to 2009, which is displayed in Fig. 3.

Because the Yangtze River Delta region has a subtropical monsoon climate with distinctive seasons, the

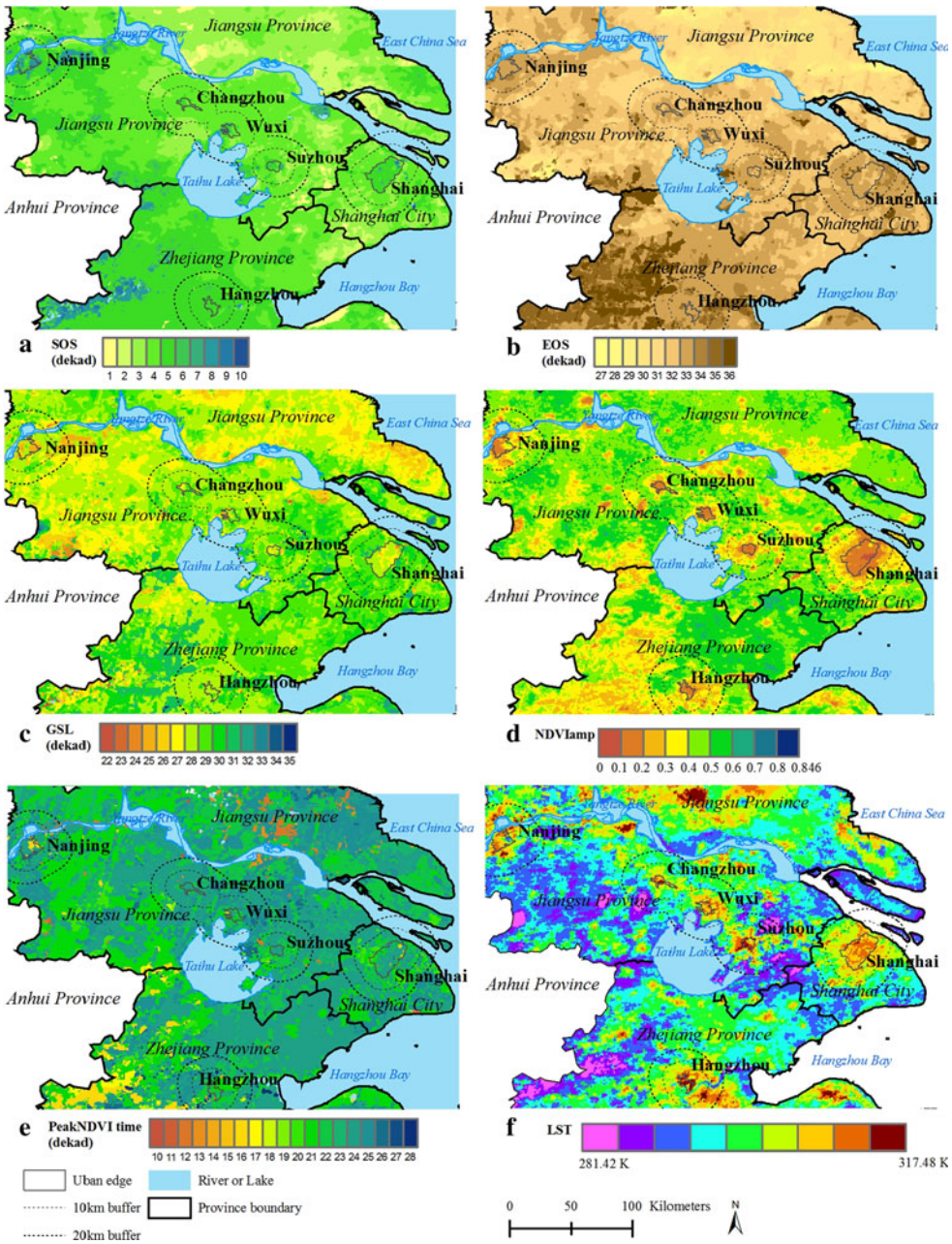

Fig. 3 Mean land surface phenological measures and mean LST in Yangtze River Delta, China. The legend refers to day-of-year (DOY). **a** SOS, **b** EOS, **c** GSL, **d** $NDVI_{amp}$, **e** the time of peak NDVI, and **f** LST. In order to avoid too many overlapping, only 8-km buffer and 20-km buffer around each urban edge are overlaid. In addition, the LST is the mean of multi-year annual maximum LSTs. In addition, to avoid possible impact of river, the area across the Yangtze River in Nanjing and Shanghai were excluded when land surface phenology and LST were extracted by buffer zones

temperature is markedly different in different seasons. To compare the difference between urban and rural areas in a year, the average LST value is calculated in each year. Similar to the LSP, the LST used in this article is the mean of the multi-year annual maximum LST (2002–2009); this value will contribute to determine the stable and overall trend of the LST difference between urban and rural areas during the studied period.

As presented in Fig. 3f, the LST ranges from 281.42 to 317.48 K, and the average LST is 306.5 K within the whole study area, except for the river, lake and sea surfaces. The temperature of urban areas is significantly higher than that in rural areas, and the LST decreases as the distance from the urban area increases. In urban areas, however, the LST ranges between 303.86 and 316.92 K, and the average LST is 310.9 K. The average LST in urban areas is 4.4 K higher than the overall average LST in the entire study area. The LST statistics in each urban area are displayed in Table 1. Shanghai has the largest urban area, consequently, the most impervious surface among the six cities, and this city has the smallest LST change (e.g., Rang and STD) among the six cities. In contrast, Hangzhou and Nanjing are still undergoing rapid urbanization, and some rural land cover (e.g., cropland, shrubs, and woodland) still remains within these city's surrounding areas; however, heterogeneous human activities will lead to greater LST

Table 1 Statistical results of LST in each city

City name	Built-up area (km^2)	Total population (10,000 persons)	LST				
			Min (K)	Max (K)	Range (K)	Mean (K)	STD (K)
Shanghai	410	1,360	307.64	314.62	6.98	310.90	1.13
Hangzhou	78	660	306.02	316.88	10.86	312.79	2.50
Nanjing	157	596	303.86	314.18	10.32	309.51	2.25
Suzhou	59	607	307.47	314.46	6.99	312.02	1.92
Wuxi	73	453	304.28	314.56	10.28	310.71	1.62
Changzhou	59	350	308.04	316.92	8.88	311.17	1.95

The urban area and total population are all acquired from statistics in 2005

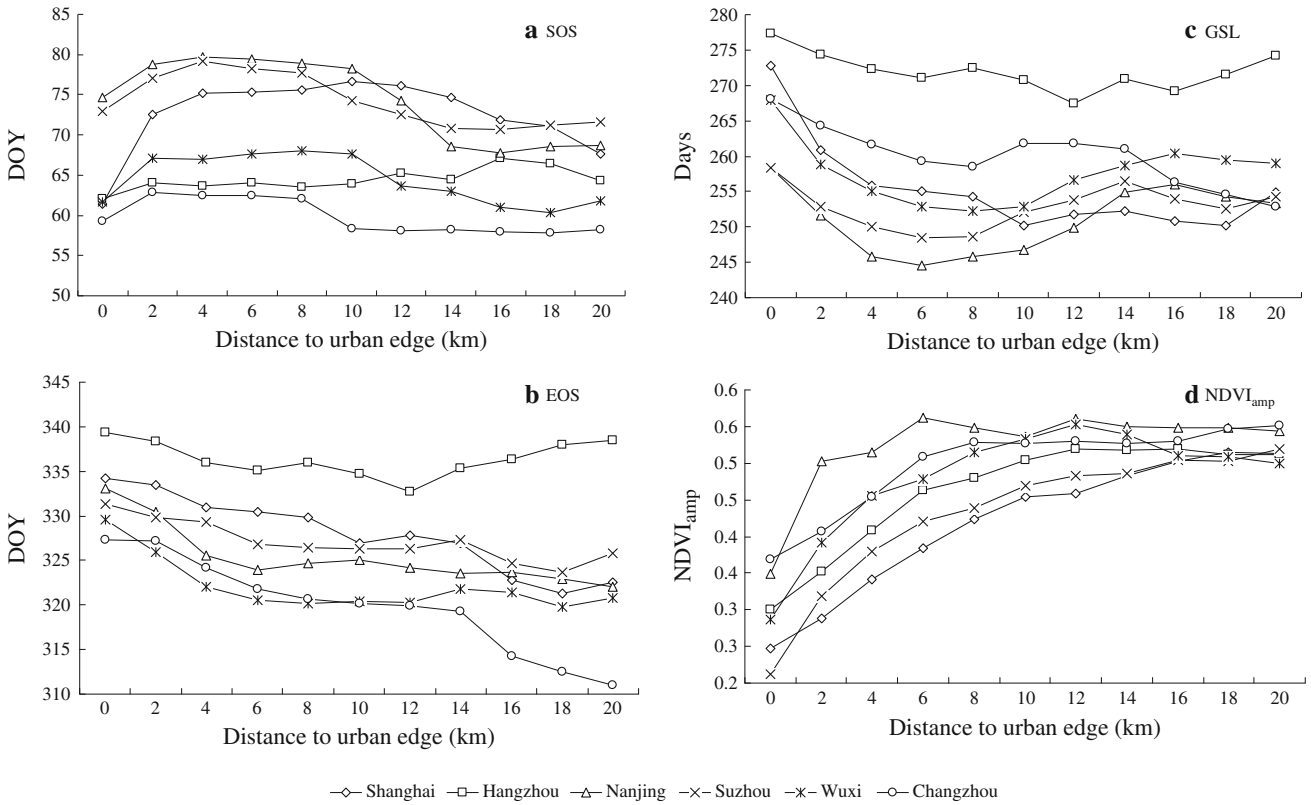

Fig. 4 Land surface phonological measures along urban–rural gradient. **a** SOS, **b** EOS, **c** GSL, and **d** $NDVI_{amp}$

ranges. In addition, the percentage of water bodies (lakes and rivers) within each city would also contribute to the LST range variation.

LSP and LST Along the Urban–Rural Gradient

In the buffer zones near the urban areas, as shown in Fig. 4, the LSP has an earlier SOS, a later EOS, a longer GSL and a lower $NDVI_{amp}$ than in outer suburbs. The SOS first increases and then decreases in all the six cities with increasing distance (Fig. 4a). In Nanjing, Shanghai, and Suzhou, vegetation in the urban areas starts to grow substantially earlier than in the buffer zones within 2 to 4 km. From 4 to 10 km, however, the SOS displays an increasing trend. In the area more than 10 km away, the SOS decreases due to minimally affected by urbanization. In Wuxi, Hangzhou, and Changzhou, vegetation in the urban areas starts to grow substantially earlier than in the buffer zone within 2 km, whereas the SOS in the buffer zones within 2 to 4 km stays constant. The SOSs of Wuxi and Changzhou start to fall in the buffer zones that are more than 8 km away. In Hangzhou, however, the SOS increases slightly and then decreases at distances greater than 14 km.

The EOS curves in the six cities show a consistently downward trend in the buffer zones within 10 km (Fig. 4b). That is, the vegetation growth finishes earlier if the growth is located further away from the urban are, whereas the vegetation growth in urban areas finishes the latest. It is worth mentioning that Hangzhou is slightly different from the other cities. The sub-tropical evergreen broad-leaved forests locating around the city and in the distant suburb have high NDVI values throughout the year, which cause a later EOS in the distant suburb and produce an obviously increasing trend beyond 12 km. For the other five cities, there are croplands beyond 12 km. Although their EOSs have consistently downward trends, small differences among them also exist because of the different crop types and farming systems.

The differences of the SOS and EOS inevitably change the GSL (Fig. 4c). Almost all of the GSL curves in the six cities show downward trends, especially within 6 km. These trends illustrate that vegetation near the urban areas has long growth durations. Almost all of the intra-annual amplitudes of the NDVI ($NDVI_{amp}$) in the six cities display upward trends near the urban edge and stable trends outside of 14 km (Fig. 4d). In the study area, the vegetation in the six cities usually presented similar low NDVIs in the winter. Therefore, the differences in the $NDVI_{amp}$ values in the six cities result from the maximal NDVI in the growth season.

Despite the differences between the six cities, the LSTs decreases monotonically with increasing distance, as shown in Fig. 5. For example, the built-up areas in Shanghai and Hangzhou are larger than in other cities, so the corresponding LSTs are obviously higher. In addition, the LSTs decrease more slowly in the three metropolises (Shanghai, Hangzhou, and Nanjing) than in the other three cities, especially Suzhou and Wuxi, due to the small built-up areas. The average LST over the six cities along the urban–rural gradient displays a monotonous declining trend, which is a remarkable logarithmic relationship with the distance in which the R^2 is 0.998: $LST = -2.222Ln(Dis) + 311.230$, where Dis is the distance to the urban edges. The statistical significance of the regression equation is determined at the 95 % level. Examinations of the scatter plots and the regression analyses all indicate potential nonlinearities in the relationships. This result shows that SUHIs exist in all six cities. Take Shanghai as an example; the average LST in the urban area is 310.9 K, the average LST in the 10-km buffer zone is 308.56 K, and the difference is 2.34 K. Similarly, the average LST in the 20-km buffer zone is approximately 3.98 K lower than in the urban area.

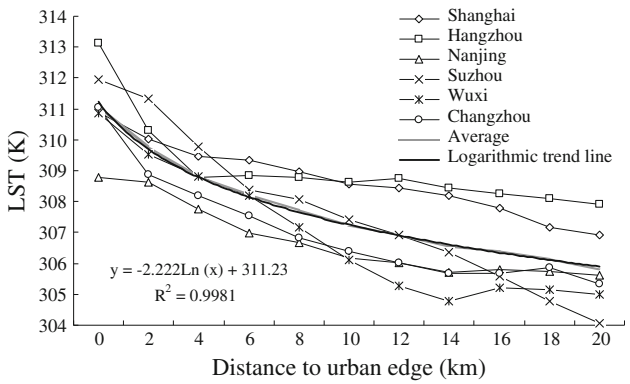

Fig. 5 LST along urban–rural gradient

Differences Between Urban Areas and the Surrounding Rural Areas

Difference in the LSP Between an Urban Area and Its Surrounding Area

Figure 6 illustrates differences between the LSPs of urban areas and those of the surrounding buffers in the six cities.

Regardless of the values of SOS, EOS, GSL, and $NDVI_{amp}$, the differences in these values between the urban area and its surrounding area are similar among the six cities. However, these trends are obviously different among the cities. In all cities except Shanghai, the ΔSOSs show similar trends within 8 km. The impact of urbanization on the phenology measures is very significant in Shanghai; the trend of ΔSOS along the urban–rural gradient is the most distinct in Shanghai among all six cities. Conversely, in Hangzhou, the ΔSOS is smaller than for the other five cities. Therefore, according to the degree of the ΔSOSs across the urban–rural gradient, the cities can be ranked as follows: Shanghai, Nanjing, Wuxi, Suzhou, Changzhou, and Hangzhou (Fig. 6a).

The ΔEOSs show similar trends along the urban–rural gradient in all six cities, especially within 6 km (Fig. 6b). These trends are consistent with those found in the literature based on remote sensing (Zhang and others 2004). However, obvious discrepancies among the six cities remain. Although the ΔEOSs in Nanjing and Wuxi are the largest among the six cities, the ΔEOSs in the other four cities do not present an obvious trend.

Although the ΔGSL trends vary between cities, there is a marked resemblance, especially within 6 km (Fig. 6c). The ΔGSL trends along the urban–rural gradient seem to be closer to the ΔEOS trends for all six cities than to the ΔSOS (Fig. 6a) trends. This result indicates that the elongated growth season length of vegetation in urban areas with intensive human activities is caused mainly by a delayed EOS. Within 6 km, according to the degree of the ΔGSLs along the urban–rural gradient, the cities can be

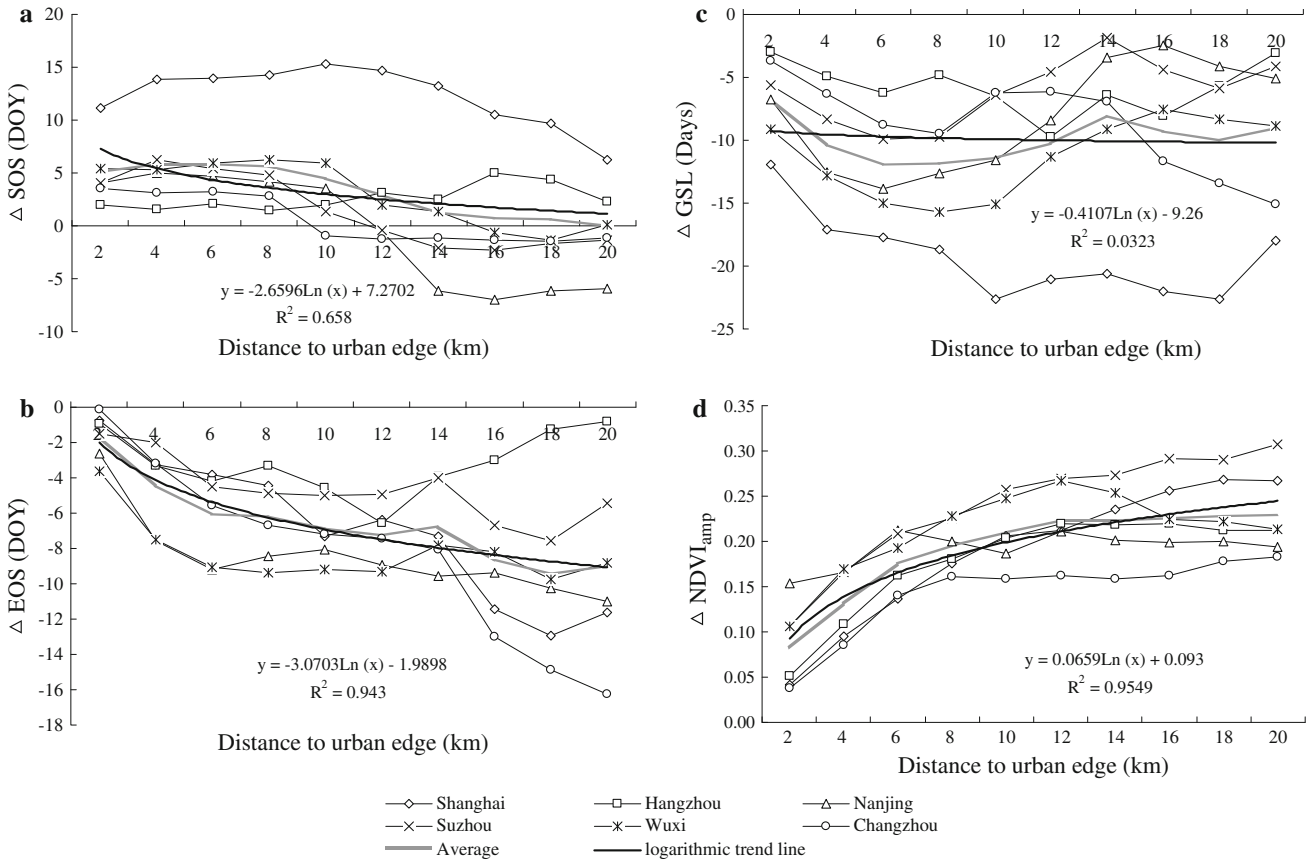

Fig. 6 The difference of land surface phonological measure between urban and its surrounding area. **a** ΔSOS, **b** ΔEOS, **c** ΔGSL, and **d** $\Delta NDVI_{amp}$

ordered as follows: Shanghai, Wuxi, Nanjing, Suzhou, Changzhou, and Hangzhou.

In the six cities, the trends of $\Delta NDVI_{amp}$ across the urban–rural gradient are all notable and are similar to those of the other three phenology measures. More remarkable changes appear in the larger cities, and the difference between the $NDVI_{amp}$ values in urban areas and in near surrounding areas is more significant than the difference between the $NDVI_{amp}$ values in urban areas and in the outer suburbs. Because $NDVI_{amp}$ is a record of the vegetation in the most vigorous growth season, the trend of $\Delta NDVI_{amp}$ reveals that the vegetation vigor in urban areas is less than that in rural areas.

The values of ΔSOS, ΔEOS, and $\Delta NDVI_{amp}$ for all six cities have a significant logarithmic relationship with the distance. The three logarithmic trends all have high statistical significances with R^2 values that are greater than 0.9 ($P < 0.01$), as shown in Fig. 6a, b, d. Although the averaged ΔSOS of all six cities has a significant logarithmic relationship with the distance, the R^2 is only 0.685 ($P < 0.01$). From Fig. 6a, the averaged ΔSOS trend line across the urban–rural gradient can be seen to be very flat within 8 km and significantly decreased beyond this distance. The ΔSOS trend along the urban–rural gradient demonstrates that the impact of the urbanized area on the SOS is stronger than the impact on the EOS, GSL, and $NDVI_{amp}$. In other words, the SOS is more sensitive to urbanization than the other three phenology measures. Although the average ΔEOS of all six cities shows no significant logarithmic relationship with the distance, there is an approximately linear correlation between the ΔEOS and the distance.

Difference of the LST Between Urban Areas and the Surrounding Rural Areas

As displayed in Fig. 7, the LST differences between urban areas and the surrounding areas (ΔLST) show that there are similar downward trends along the urban–rural gradients in all six cities. Once again, obvious UHI effects exist in all six cities. Although Hangzhou is the capital of the Zhejiang province and its urban area is larger than those of Suzhou, Wuxi, and Changzhou, the LST in the urbanized area is much higher than in the suburbs due to the large vegetated area around the urban area. Consequently, the ΔLST trend line is lower than for other cities. Overall, the averaged

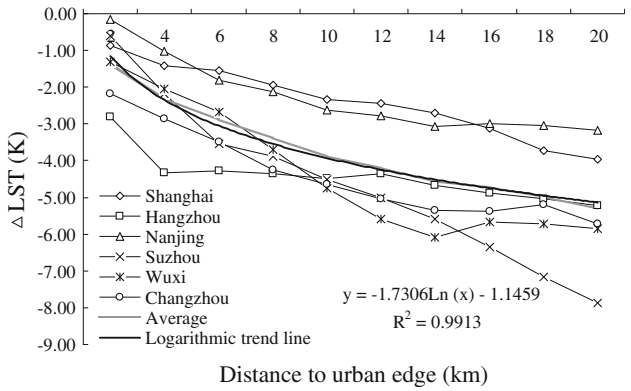

Fig. 7 The difference of LST (ΔLST) between urban and its surrounding area

ΔLST presents a monotonous downtrend, with a significant logarithmic trend and a maximum R^2 of 0.9913 ($P < 0.01$) along the urban–rural gradient.

Relationship Between the LSP and LST Along the Urban–Rural Gradient

The UHI, as an important result of urbanization, is analyzed coupled with the LSP along the urban–rural gradient. The mean LSPs and mean LSTs of all six cities in each buffer are extracted. Figure 8 shows the scatter diagrams of the relationship between the two. The SOS and LST have different trends along the urban–rural gradient, which can be fit with a quadratic equation (Fig. 8a, $P < 0.01$). The trends in these parameters seem difficult to be explained by natural processes. In fact, the LST appears to decrease monotonically as the distance increases (Fig. 7); however, the SOS only decreases within 6 km. When the distance exceeds 6 km, LST decreases gradually as the amounts of native vegetation and crops increases. In other words, the effect of urbanization on the SOS only extends to 6 km, whereas the effect on the LST extends further from the urban edge.

Unlike the SOS, the relationship between the EOS and the LST corresponds to a significant linear equation (Fig. 8b, $P < 0.01$) along the urban–rural gradient. This relationship can be explained as follows: the EOS and LST all decrease monotonically as the distance increases, and there is a strong and positive correlation between both variables, which implies that the effects of urbanization on the SOS and LST are consistent and extend far from the urban edge.

Apparently the nonlinear relationship of SOS with LST leads to nonlinear relationship of GSL with LST. Figure 8c shows that there is a significant negative quadratic relationship ($P < 0.01$) between the GSL and the LST along the urban–rural gradient. This relationship is similar to the relationship between the SOS and the LST because the GSL is the difference between the SOS and the EOS. Similarly, there is a strong and positive correlation between the GSL and the LST only within 6 km. However, 6 km away, the relationship between the GSL and the LST might not be related to urbanization. Comparing Fig. 8a with Fig. 8b reveals that the relationship between the GSL and the LST is primarily influenced by the SOS.

The $NDVI_{amp}$ is strongly correlated with the LST along the urban–rural gradient (Fig. 8b); moreover, there is a significant negative correlation coefficient with a maximum value of -0.971 ($P < 0.01$). This result indicates that a higher LST decreases the vegetation growth peak value during the growth period in an urban area and its near surrounding area to a greater extent than in the outer suburbs. Physiologically, the warmer microclimates induced by an UHI would inhibit the photosynthetic capacity of vegetation within urban areas during the summer (Imhoff and others 2004). That is, a higher LST may weaken the seasonal characteristic of land surface vegetation (e.g., an increasing number of evergreen plants are being planted in urbanized areas). The growth peak value actually decreases, although there is a longer growth season. In addition, there is a well-fitted linear curve with a maximum R^2 of 0.9429 ($P < 0.01$) between the $NDVI_{amp}$ and the LST along the urban–rural gradient.

The relationship between the LSP and the LST shows that the LSP is highly correlated with the LST along the urban–rural gradient, especially within 6 km. In addition, the UHI effect is a primary result of urbanization. This finding shows that urbanization affects the LSP at a maximum distance of 6 km. In fact, the UHI is mainly created by the human activity (Yue and others 2010; Buyantuyev and Wu 2010). There is a high population density and intensive human activities denoted by the GDP per square kilometer in and near the urbanized area. Similar to the difference in the phenological measures and the LST along the urban–rural gradient, the differences between the population density (ΔPOP) and between the GDP (ΔGDP) per square kilometer in an urbanized area and each buffer zone are extracted. The results show that both the ΔPOP and the ΔGDP correlate strongly with the distance according to a significant logarithmic relationship ($R^2 > 0.8$, $P < 0.01$), as displayed in Fig. 9a, b, and the trends of the ΔPOP and the ΔGDP are similar to the trend of the ΔLST along the urban–rural gradient (Fig. 7).

Along the urban–rural gradient, there is a strong positive correlation coefficient of up to 0.86 ($P < 0.01$) between the ΔPOP and the ΔGSL and a strong negative correlation coefficient of up to -0.93 ($P < 0.01$) between the ΔPOP and the $\Delta NDVI_{amp}$. Similarly, there is a strong positive correlation coefficient of up to 0.86 ($P < 0.01$) between the ΔGDP and the ΔGSL and a strong negative correlation coefficient of up to -0.95 ($P < 0.01$) between the ΔGDP

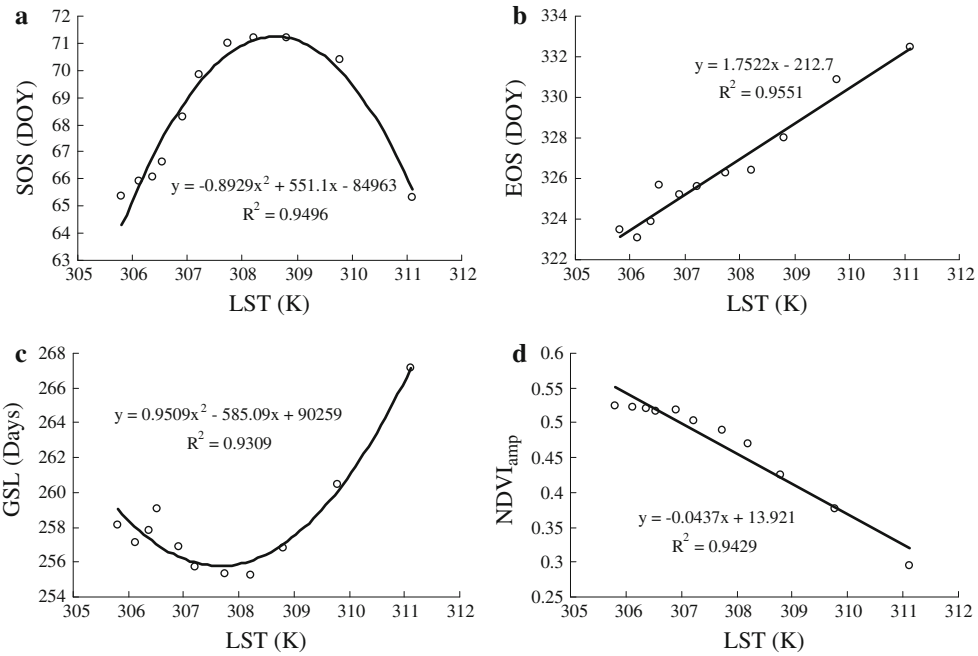

Fig. 8 Scatter diagrams along urban–rural gradient: **a** LST versus SOS, **b** LST versus EOS, **c** LST versus GSL, and **d** LST versus $NDVI_{amp}$

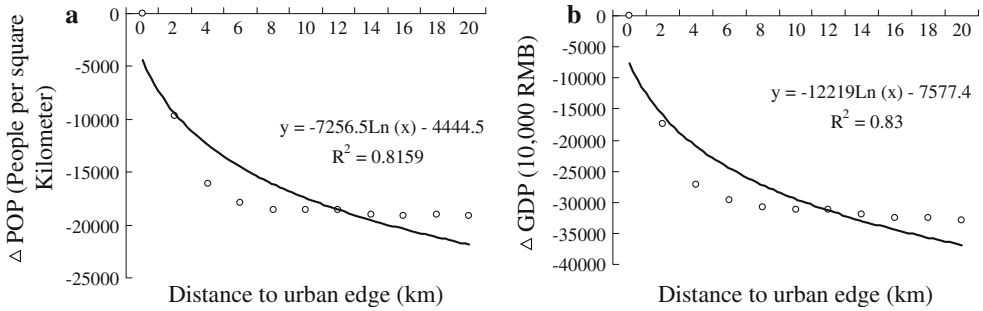

Fig. 9 Fitted curves of ΔPOP and ΔGDP along urban–rural gradient. **a** Fitted curve between ΔPOP and the distance to the urban edge, and **b** fitted curve between ΔGDP and the distance to the urban edge

and the $\Delta NDVI_{amp}$ along the urban–rural gradient. These significant correlation coefficients demonstrate that human activities associated with the urbanization process have considerable influence on the growth season and vigor of land surface vegetation in an urban area and its surrounding area. Overall, the influence is similar in all six cities in the Yangtze River Delta.

Discussion

Spatial Difference of the LSP Among the Cities

The LSP was dominated by various factors, such as the land use/land cover, the temperature, and the precipitation at regional scale. In particular, the spatial distribution of the land use/land cover varies in the study area. For example, a large area of crops covers the areas north of the Yangtze River in the Jiangsu province; in contrast, a large area of sub-tropical evergreen broadleaf forest clusters in the Zhejiang province. To view the spatial pattern as a whole, nearer to water (e.g., Taihu Lake, Yangtze River, and East China Sea), the land surface vegetation revives earlier (i.e., a smaller SOS), and the dormancy onset occurs later (i.e., a larger EOS). Unlike the other cities, Nanjing and Hangzhou have more forests in their urban areas and the surrounding areas; therefore, Nanjing and Hangzhou do not seem to show earlier SOSs compared with the urban areas and the surrounding area (Fig. 3a). For these reasons, Nanjing and Hangzhou seem to have short GSLs compared to the urban areas and the surrounding areas (Fig. 3c). The $NDVI_{amp}$ provides the best contrast between the urban and rural areas (Fig. 3d). The times of the peak NDVI of the LSP do not appear to be obviously different between the

urban areas and the surrounding areas (Fig. 3e) due to various factors such as the vegetation communities, the soil condition, and the aerial pollution.

Differences in the LSP Trend Along the Urban–Rural Gradient Among the Cities

In general, we can hypothesize that the effect of urban development on the LSP is stronger near urban areas and decreases gradually toward rural areas (Zhang and others 2004). However, the effect exists only within 6 km because the land cover is different between the suburbs near the urban area and the outer suburbs that have more crops with special phenology cycles. The Fig. 10 shows the percentage of crop area, derived from MODIS land cover product, in each buffer zone. Crop area in the near buffer zones is small, especially in three metropolises within 6 km. Beyond 6 km, however, crop area increase apparently. When distance increases beyond 12 km, crop area increases rapidly. These variation change points of crop area are consistent to those change points of SOS along urban–rural gradient. In this study area, the main crop is winter wheat, rice, and corn (Zhou and Zhou, 2009). Winter wheat starts to growth earlier than vegetation in urban and its near surrounding area, and has high NDVI in spring, and consequently, affects the SOS and ΔSOS trends (Figs. 4a, 6a) along the urban–rural gradient. After winter wheat is harvested, rice and corn are planted in June and growth continued until the mid-autumn. And their earlier ending time of growth than secondary vegetation leads to the downward trends of EOS (Fig. 4b).

The LSP displays a similar trend in the suburbs near the urban areas in almost all of the cities (Fig. 4). Moreover, the urbanization has different degrees of influence on the LSP. Except for the GSL, the other three trends are clear and easily recognizable among the six cities within 8 km. Beyond this distance, the LSP shows an irregular and unclear trend resulted from increasing crop area. The LSP trend differs among the cities. For example, as listed in Table 1, although Shanghai is approximately seven times

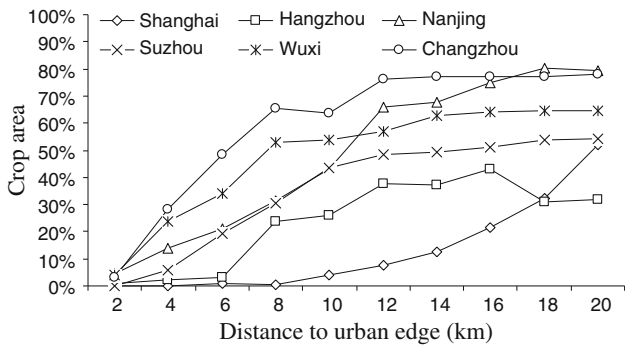

Fig. 10 The percentage of crop area in each buffer zone

larger than Suzhou, the population density of Suzhou is greater than that of Shanghai. This result implies that the two cities would exert a similar effect on the phenology of the surrounding vegetation. Although Changzhou is the same size as Suzhou and the former's population density is larger than the latter's, the SOS trend is obviously different between the two. Although we can deduce that the influence of urbanization in a large city may be larger than that in a small city, the influence of urbanization on the LSP is a result of the concerted action of manifold factors, such as the land use/land cover, the urban district area, the population density, industrial production, the economic development level and other unknown factors. Nevertheless, these factors act upon one another. For example, the SOS curves in the six cities (Fig. 4a) have similar trends, but these trends are different in the buffer zones from 2 to 10 km, in which the phenology measures are not only influenced by the urban size, population, and diversity but also by the types and quantity of vegetation. For instance, the vegetation in the urban areas and the surrounding areas with radii of approximately 4 km in Nanjing, Shanghai, and Suzhou city has an obviously early SOS due to the larger urban size, larger population, and rapid urbanization; however, the vegetation has an obviously early SOS within 2 km of Wuxi and Changzhou due to the relatively small urban size and population. In addition, the SOS maintains an approximately steady trend in Hangzhou because of the plentiful natural secondary forest existing around the urban area despite the large urban size and population. The GSL, however, appears to have a regular trend only within 6 km for all six cities. This result shows that vegetation in urban areas and the near surrounding areas germinate and leaf out early and that the fall of its leaves is delayed in autumn and winter because of the changed urban climate resulting from the effects of human activities, such as the heat island effect. Although the GSL is the difference between the SOS and the EOS, the GSL trend (Fig. 4c) is not derived from the trends of the SOS and EOS. It is apparent that the GSL is influenced and controlled by more factors. The $NDVI_{amp}$ in urban areas is less than that in the surrounding areas. These patterns can be explained by two primary factors. One factor is that urban areas contain proportionally less fractional vegetation cover, which leads to a reduced NDVI signal. Another factor is that the land cover transformations and human activities in an urban area modify the hydrological regime and vegetation species composition and produce UHIs and air pollution, which would reduce the vegetation vigor (Honour and others 2009).

The LSP difference between an urban area and its surrounding area is used to measure the degree of change along the urban–rural gradient. To a certain extent, the degree of the LSP change can be regarded as a creation of

the urbanization. It is well known that vegetation growth is mainly controlled by the water and heat conditions (Daniels and Vablen 2003). Many artificial buildings in an urbanized area result in a large number of impervious surfaces, which increase the frequency and magnitude of floods downstream, lower the groundwater recharge and alter the hydrologic regime and further deteriorate the aquatic and the adjacent riparian ecosystems (Sung and Li 2012). The effect of impervious surfaces is not only limited to the urban stream but also increases the sensible heat flux at the expense of latent heat flux. At the same time, UHI effects are exacerbated by the anthropogenic heat generated by traffic, industry, and domestic buildings, impacting the local climate through the city's compact mass of buildings that affects the exchange of energy and the levels of conductivity (Yuan and Bauer 2007). The UHI effect increases the ambient temperatures as buildings and other impervious surfaces, as well as pervious surfaces, capture solar energy. Oke (1973) suggested that the UHI intensity is related to the logarithm of the population. In fact, the influence of urbanization on human health, the ecosystem function, the local weather and possibly the climate is positively related to the urban size, including the urbanized area and the population.

Comparing the ΔSOS with the ΔEOS, the latter has a more complex variation among cities than the former. This finding seems to indicate that the impact of urbanization on the ΔEOS is complex. For example, Shanghai has the largest area and population, but its ΔEOS is not the largest among the six cities. The medium-sized city of Wuxi, however, has the largest ΔEOS. The difference in the ΔEOS trend among the cities reveals that the influence of urbanization on the EOS is a consequence of many factors. For instance, urban land cover transformations affect plant phenology most directly by modifying the hydrological regime, the UHI, the local and regional climates, and the vegetation cover and species composition. Urban hydrology, characterized by increased runoff and reduced groundwater (Pickett and others 2011; Buyantuyev and Wu 2012), is likely to have significant repercussions for phenology in urban areas. Urban vegetation frequently includes exotic species that may exhibit phenology patterns that are different from those of native plants. Furthermore, some plants delay their flowering (Neil and others 2010), which would delay the EOS.

In addition, the GSL is the difference between the SOS and the EOS. The ΔGSL is also complicated, especially beyond 6 km. The GSL is shown to be affected and controlled by the EOS to a greater extent than by the SOS. Among the six cities, Shanghai, Wuxi, and Nanjing have obvious changes in the ΔGSL between the urban areas and the surrounding areas that resulted from significant changes in the human activities along the urban–rural gradient (Fig. 6c). In Hangzhou, however, abundant sub-tropical evergreen broad-leaved forests distributed around the urban area result in an inconspicuous difference between the GSL of the urban area and that of its surrounding area. On the one hand, the $\Delta NDVI_{amp}$ trend implies that urbanization reduces the vegetation vigor in the urban area and its near surrounding area. Possible reasons might be that the large amount of impermeable land surface in urban areas obstructs the water cycle between the vegetation and the soil, and vegetation photosynthesis is weakened by dust and pollutants in the atmosphere. On the other hand, less vegetation in the urban area and its near surrounding area is another important factor leading to small $NDVI_{amp}$.

Through the above analysis, we found that urbanization simultaneously lengthens the GSL and reduces the $NDVI_{amp}$. In spite of a longer growing season, reductions in the peak vegetation activity in urban areas suggest that urban productivity is likely lower than in rural areas and may be used as a surrogate for the effects of global warming on plant phenology. In addition, a 1-day extension of the GSL was associated with an approximately 2 % increase in the net ecosystem exchange of carbon, and extensive reductions in $NDVI_{amp}$ could reduce the urban NPP despite the observed longer growing season (White and others 2002). However, Imhoff and others (2004) found that the urbanization actually increases the NPP during the winter months in cold regions, followed by a pronounced decrease during the summer. The gain in the winter NPP is a result of a localized "urban warming," which extends the growing season in proximity to urban areas. Whether the urbanization increases or decreases the NPP in this study area requires further study.

Relationship Between the LSP and the LST Along the Urban–Rural Gradient

Higher population density leads to large amounts of waste heat in the urban areas. In addition, high-intensity urban construction in urban areas has dramatically changed the surface structure, which disrupts the original hydrologic cycle and the heat balance between the surface air, the land surface and the shallow soil. Large areas of impervious surface and high population densities directly lead to and exacerbate the UHI effect in urban areas. Along the urban–rural gradient, there is a strong positive correlation between LST and POP with a coefficient up to 0.89 ($P < 0.01$). Similarly, the LST is strongly correlated with GDP with a coefficient up to 0.90 ($P < 0.01$). These strong correlations indicate that high population densities and intensive economic production are the leading causes of UHIs during the rapid urbanization process in developing countries. For the SOS, the relationship with the LST can be reasonably explained within 6 km. When the distance increases to

6 km, the LST decreases gradually from 311.11 to 308.22 K; at the same time, the SOS increases gradually from 65.33 to 71.21 DOY, and the relationship can be described by a significant linear correlation. Obviously, increasing crop area leads to the nonlinear relationship when the distance to urban edges exceeds 6 km (Fig. 10). In addition, the EOS decreases gradually from 332.47 to 326.42 DOY within this distance. Moreover, the relationship between the EOS and the LST is also a significant linear correlation over the whole urban–rural gradient from the urban area to the far suburb area (20 km). The relationship between the GSL and the LST is the result of the integration of the above two relationships and shows that this relationship is credible only within 6 km. The relationship between the $NDVI_{amp}$ and the LST is also significant along the whole gradient. The $NDVI_{amp}$ increases gradually with decreasing LST from the urban area to its surrounding area. In summary, there is a strong correlation between the LSP and the LST along the urban–rural gradient, especially within 6 km.

Although the LST, as an important effect of urbanization, has a great impact on the LSP, the relationship between the SOS and the LST, as well as the GSL, reveals that the LSP is also influenced by many element: (1) increasing impervious surface area in urban areas, which changes the original water cycle in both the soil and the air, the soil structure and the organic matter content; (2) in urban and sub-urban areas, the landscape and structure of vegetation is changed due to the increasing introduction of exotic tree species; (3) pollutants in the atmosphere, water body and soil directly damage the structures of stems roots and leaves and thus reduce the vegetation photosynthesis in urban areas; and (4) pollutants and suspended particulates in the atmosphere reduce the solar radiation absorbed by vegetation.

In fact, the air temperature and the water cycle are two of the most important environmental factors impacting plant growth processes. Moreover, the accumulated temperature and soil moisture directly determine the rhythm of plant growth. Although the surface temperature is different from the air temperature, the potential relationship between the LST and the air temperature has been explored by many studies (Mostovoy and others 2005; Riddering and Queen 2006; Cristóbal and others 2008; Zhang and others 2011). These studies reveal that the SUHI and UHI tend to co-vary spatially and temporally. Specifically, the LST displays a stronger dependence on microscale site characteristics than the air temperature (Arnfield 2003; Nichol 1996). The LST controls the surface heat and water exchange with the atmosphere (Yuan and Bauer 2007). This result implies that the surface temperature directly or indirectly increases the accumulated temperature, which causes the plants to begin growing earlier and to cease growing later in urban areas than in rural areas. Naturally, the GSL is longer in urban areas than in rural areas, especially within 6 km, and has a significant statistical relationship with the LST.

Conclusion

Through the analysis of LSP measures along the urban–rural gradient, we found that urbanization in the Yangtze River Delta advances the SOS, postpones the EOS, prolongs the GSL, and reduces the $NDVI_{amp}$. The conclusion is consistent with research conducted by White and others (2002) and de Beurs (2005). Overall, urbanization has a greater impact on the LSP nearer to the urban area, especially within 6 km. The extension of the impact, however, varies because of the variation in urban size, urban function and local vegetation types and spatial distribution. The influence of urbanization on the EOS and the $NDVI_{amp}$ is more obvious than that on the SOS and the GSL. In addition, surface UHIs generally exist in the six cities, and the LST declines gradually along the urban–rural gradient according to a significant logarithmic relationship with the distance, especially within 6 km to the urban edge. From the view point of the averaged values of the six cities, the difference between the LSP in the urban area and that in its surrounding area is a significant logarithmic relationship with the distance; the ΔGSL does not follow this relationship. There is also a very strong linear relationship between the LSP and the LST along the urban–rural gradient, especially within 6 km. Combining the LSP trend with its relationship with the LST along the urban–rural gradient, we conclude that the influence of urbanization on the LSP extends to a maximum distance of 6 km from the urban edge. In addition, the UHI, combined with other factors, induces an earlier SOS, a later EOS, a longer GSL, and a lower $NDVI_{amp}$ in urban areas and the near surrounding areas. In addition, the correlations between LSP and GDP and population density along the urban–rural gradient reveal that human activities have considerable influence on the growth season and vigor of land surface vegetation in an urban area and its surrounding area.

Acknowledgments The study was financially supported by the National Natural Science Foundation of China (Grant No. 41001364) and the Specialized Research Fund for the Doctoral Program of Higher Education of China (Grant No. 20090191120030). We thank Dr. ZW Sun for his constructive comments and suggestions on our manuscript. And we are very grateful for thorough and helpful comments from reviewers of the manuscript.

References

Ahas R, Aasa A, Menzel A, Fedotova VG, Scheifinger H (2002) Changes in European spring phenology. Int J Climatol 22:1727–1738

Arnfield AJ (2003) Two decades of urban climate research: a review of turbulence, exchanges of energy and water, and the urban heat island. Int J Climatol 23:1–26

Atkinson PM, Jeganathan C, Dash J, Atzberger C (2012) Inter-comparison of four models for smoothing satellite sensor time-series data to estimate vegetation phenology. Remote Sens Environ 123:400–417

Beck PSA, Atzberger C, Hogda KA, Johansen B, Skidmore AK (2006) Improved monitoring of vegetation dynamics at very high latitudes: a new method using MODIS NDVI. Remote Sens Environ 100:321–334

Buyantuyev A, Wu J (2010) Urban heat islands and landscape heterogeneity: linking spatiotemporal variations in surface temperatures to land-cover and socioeconomic patterns. Landsc Ecol 25:17–33

Buyantuyev A, Wu J (2012) Urbanization diversifies land surface phenology in arid environments: interactions among vegetation, climatic variation, and land use pattern in the Phoenix metropolitan region, USA. Landsc Urban Plan 105:149–159

Chen J, Jönsson P, Tamura M, Gu ZH, Matsushita B, Eklundh L (2004) A simple method for reconstructing a high-quality NDVI time-series data set based on the Savitzky–Golay filter. Remote Sens Environ 91:332–344

Cristóbal J, Ninyerola M, Pons X (2008) Modeling air temperature through a combination of remote sensing and GIS data. J Geophys Res 113:1–13

Daniels LD, Vablen TT (2003) Regional and local effects of disturbance and climate on altitudinal treelines in northern Patagonia. J Veg Sci 14:733–742

Dash J, Jeganathan C, Atkinson PM (2010) The use of MERIS terrestrial chlorophyll index to study spatio-temporal variation in vegetation phenology over India. Remote Sens Environ 114: 1388–1402

de Beurs KM (2005) A statistical framework for the analysis of long image time series: the effect of anthropogenic change on land surface phenology. Dissertation, University of Nebraska-Lincoln, pp 31–32

de Beurs KM, Henebry GM (2010) Phenological research: methods for environmental and climate change analysis. In: Hudson IL, Keatley MR (eds) Phenological research. Springer, New York, pp 177–207. doi:10.1007/978-90-481-3335-2_9

Fisher JI, Mustard JF, Vadeboncoeur MA (2006) Green leaf phenology at Landsat resolution: scaling from the field to the satellite. Remote Sens Environ 100:265–279

Garrity SR, Bohrer G, Maurer KD, Mueller KL, Vogel CS, Curtis PS (2011) A comparison of multiple phenology data sources for estimating seasonal transitions in deciduous forest carbon exchange. Agric For Meteorol 151:1741–1752

Ge QS, Dai JH, Zheng JY (2010) The progress of phenology studies and challenges to modern phenology research in China. Bull Chin Acad Sci 25(3):310–316

Gong JZ, Xia BC, Li N, Guo L (2006) Effects of spatial grain size on landscape pattern of land-cover types in the rapidly urbanized region. Acta Ecol Sin 26(7):2198–2206

Griguolo S, Mazzanti M (2004) Using a feed-forward neural network to simulate missing values in SPOT/VEGETATION NDVI images. In: Proceedings of the 2nd international VEGETATION user conference

Han GF, Xu JH (2008) Spatio-temporal correlation between urbanization and vegetation vigor in the Delta of Yangtze River. Ecol Sci 27(1):1–5

Han GF, Xu JH, Yuan XZ, Wang ZH (2007) Spatiotemporal change of vegetation distribution in central area of Chongqing City in 1988–2001. Chin J Ecol 26(9):1412–1417

Honour SL, Bell JNB, Ashenden TW, Cape JN, Power SA (2009) Responses of herbaceous plants to urban air pollution: effects on growth, phenology and leaf surface characteristics. Environ Pollut 157:1279–1286

Hudson Dunn AD, de Beurs KM (2011) Land surface phenology of North American mountain environments using moderate resolution imaging spectroradiometer data. Remote Sens Environ 115:1220–1233

Hufkens K, Friedl M, Sonnentag O, Braswell BH, Milliman T, Richardson AD (2012) Linking near-surface and satellite remote sensing measurements of deciduous broadleaf forest phenology. Remote Sens Environ 117:307–321

Imhoff ML, Bounoua L, DeFries R, Lawrence WT, Stutzer D, Tucker CJ, Ricketts T (2004) The consequences of urban land transformation on net primary productivity in the United States. Remote Sens Environ 89:434–443

Imhoff ML, Zhang P, Wolfe RE, Bounoua L (2010) Remote sensing of the urban heat island effect across biomes in the continental USA. Remote Sens Environ 114:504–513

Ivits E, Cherlet M, Tóth G, Sommer S, Mehl W, Vogt J, Micale F (2012) Combining satellite derived phenology with climate data for climate change impact assessment. Glob Planet Change 88–89:85–97

Jönsson AM, Eklundh L, Hellström M, Bärring L, Jönsson P (2010) Annual changes in MODIS vegetation indices of Swedish coniferous forests in relation to snow dynamics and tree phenology. Remote Sens Environ 114:2719–2730

Karlsen SR, Hogda KA, Wielgolaski FE, Tolvanen A, Tømmervik H, Poikolainen J, Kubin E (2009) Growing-season trends in Fennoscandia 1982–2006, determined from satellite and phenology data. Clim Res 39:275–286

Kinzig AP, Warren P, Martin C, Hope D, Katti M (2005) The effects of human socioeconomic status and cultural characteristics on urban patterns of biodiversity. Ecol Soc 10:23–35

Lee S, French SP (2009) Regional impervious surface estimation: an urban heat island application. J Environ Plan Manag 52:477–496

Li JS, Gao JX, Zhang XL, Zheng XM (2005) Effects of urbanization on biodiversity: a review. Chin J Ecol 24(8):953–957

Li RP, Zhou GS, Zhang HL (2006) Research advances in plant phenology. Chin J Appl Ecol 17(3):541–544

Lo C, Quattrochi D (2003) Land-use and land-cover change, urban heat island phenomenon, and health implications: a remote sensing approach. Photogramm Eng Remote Sens 69:1053–1063

Maignan F, Bréon FM, Bacour C, Demarty J, Poirson A (2008) Interannual vegetation phenology estimates from global AVHRR measurements Comparison with in situ data and applications. Remote Sens Environ 112:496–505

McDonnell MJ, Pickett STA, Groffman P, Bohlen P, Pouyat RV, Zipperer WC, Parmelee RW, Carreiro MM, Medley K (1997) Ecosystem processes along an urban-to-rural gradient. Urban Ecosyst 1:21–36

Mostovoy GV, King R, Reddy KR, Kakani VG (2005) Using MODIS LST data for high-resolution estimates of daily air temperature over Mississippi. In: Proceedings of the 3rd international workshop on the analysis of multi-temporal remote sensing images, pp 76–80

Neil K, Wu JG (2006) Effects of urbanization on plant flowering phenology: a review. Urban Ecosyst 9:243–257

Neil KL, Landrum L, Wu J (2010) Effects of urbanization on flowering phenology in the metropolitan phoenix region of USA: findings from herbarium records. J Arid Environ 74:440–444

Nichol JE (1996) High-resolution surface temperature patterns related to urban morphology in a tropical city: a satellite-based study. J Appl Meteorol Clim 35:135–146

Oke TR (1973) City size and the urban heat island. Atmos Environ 7:769–779

Pettorelli N, Vik JO, Mysterud A, Gaillard JM, Tucker CJ (2005) Using the satellite-derived NDVI to assess ecological responses to environmental change. Trends Ecol Evol 20:503–510

Pickett STA, Cadenasso ML, Grove JM et al (2011) Urban ecological systems: scientific foundations and a decade of progress. J Environ Manag 92:331–362

Pouliot D, Latifovic R, Fernandes R, Olthof I (2011) Evaluation of compositing period and AVHRR and MERIS combination for improvement of spring phenology detection in deciduous forests. Remote Sens Environ 115:158–166

Reed BC, Brown JF, Vanderzee D, Loveland TS, Merchant JW, Ohlen DO (1994) Measuring phenological variability from satellite imagery. J Veg Sci 5:703–714

Riddering JP, Queen LP (2006) Estimating near-surface air temperature with NOAA AVHRR. Can J Remote Sens 32:33–43

Roetzer T, Wittenzeller M, Haeckel H, Nekovar J (2000) Phenology in central Europe-differences and trends of spring phenophases in urban and rural areas. Int J Biometeorol 44:60–66

Roth M, Oke TR, Emery WJ (1989) Satellite-derived urban heat islands from three coastal cities and the utilization of such data in urban climatology. Int J Remote Sens 10:1699–1720

Sailor D (1995) Simulated urban climate response to modifications in surface albedo and vegetative cover. J Appl Meteorol Clim 34:1694–1704

Sakamoto T, Wardlow BD, Gitelson AA, Verma SB, Suyker AE, Arkebauer TJ (2010) A two-step filtering approach for detecting maize and soybean phenology with time-series MODIS data. Remote Sens Environ 114:2146–2159

Smith PM, Kalluri SNV, Prince SD, DeFries RS (1997) The NOAA/NASA pathfinder AVHRR 8-km land dataset. Photogramm Eng Remote Sens 63:12–31

Soudani K, Hmimina G, Delpierre N et al (2012) Ground-based network of NDVI measurements for tracking temporal dynamics of canopy structure and vegetation phenology in different biomes. Remote Sens Environ 123:234–245

Sung CY, Li MH (2012) Considering plant phenology for improving the accuracy of urban impervious surface mapping in a subtropical climate regions. Int J Remote Sens 33:261–275

Tucker CJ, Pinzon JE, Brown ME et al (2005) An extended AVHRR 8-km NDVI dataset compatible with MODIS and SPOT vegetation NDVI data. Int J Remote Sens 26:4485–4498

Voogt JA, Oke TR (2003) Thermal remote sensing of urban climates. Remote Sens Environ 86:370–384

Wang YJ, Li JX, Wu JP, Song YC (2006a) Landscape pattern changes in urbanization of Pudong New District, Shanghai. Chin J Appl Ecol 17(1):36–40

Wang WJ, Shen WM, Liu XM, Zhang F, Pan YZ, Luo HJ (2006b) Research on the relation of the urbanization and urban heat island effect changes in Beijing based on remote sensing. Res Environ Sci 19(2):44–48

Weier J (2002) Urbanization's aftermath. http://earthobserva-tory.nasa.gov/Study/Lights3/lights_carbon.html. Accessed 26 June 2007

White MA, Thornton PE, Running SW (1997) A continental phenology model for monitoring vegetation responses to interannual climatic variability. Glob Biogeochem Cycles 11:217–234

White MA, Nemani RR, Thornton PE, Running SW (2002) Satellite evidence of phenological differences between urbanized and rural areas of the Eastern United States deciduous broadleaf forest. Ecosystems 5:260–273

White MA, de Beurs KM, Didan K et al (2009) Intercomparison, interpretation and assessment of spring phenology in North America estimated from remote sensing for 1982–2006. Glob Change Biol 15:2335–2359

Wu YF, Li MS, Li J (2008) Research on a detection method of Chinese terrestrial vegetation greenness periods based on remote sensing. J Remote Sens 12(1):92–103

Xu WT, Wu BF, Yan CZ, Huang HP (2005) China land cover 2000 using SPOT VGT S10 data. J Remote Sens 9(2):204–214

Yuan F, Bauer M (2007) Comparison of impervious surface area and normalized difference vegetation index as indicators of surface urban heat island effects in Landsat imagery. Remote Sens Environ 106:375–386

Yue WZ, Xu LH, Xu JH (2010) Thermal environment change and its socioeconomic drivers in Shanghai city during the 1990s. Acta Ecol Sin 30(1):155–164

Zhang XY, Friedl MA, Schaaf CB et al (2003) Monitoring vegetation phenology using MODIS. Remote Sens Environ 84:471–475

Zhang XY, Friedl MA, Schaaf CB, Strahler AH, Schneider A (2004) The footprint of urban climates on vegetation phenology. Geophys Res Lett 31:L12209

Zhang W, Huang Y, Yu YQ, Sun WJ (2011) Empirical models for estimating daily maximum, minimum and mean air temperatures with MODIS land surface temperatures. Int J Remote Sens 32:9415–9440

Zheng JY, Ge QS, Hao ZX (2002) Impacts of climate warming on plants phenophases in China for the last 40 years. Chin Sci Bull 47:1826–1831

Zhou SD, Zhou WK (2009) Influence and countermeasure of climate changes on agricultural production in Yangtze Delta. Acta Agric Zhejiang 21(4):307–310

Zhou L, Tucker CJ, Kaufmann RK, Slayback D, Shabanov NV, Myneni RB (2001) Variations in northern vegetation activity inferred from satellite data of vegetation index during 1981 to 1999. J Geophys Res 106:20069–20083